Mathematics

AIMS Mathematics, 11(5): 14522–14546.
DOI: 10.3934/math.2026595
Received: 26 January 2026
Revised: 07 May 2026
Accepted: 14 May 2026
Published: 22 May 2026

https://www.aimspress.com/journal/Math

Research article

Extending the 3D Dong chaotic system to a 5D hyperchaotic system with three positive Lyapunov exponents: Dynamics, multistability, offset boosting, and PSO-DE based complexity optimization

Khaled Benkouider[1], Mohammed A. Saleh[2], Aceng Sambas[3,4,5,*], Sulaiman M. Ibrahim[6], Abdulgader Z. Almaymuni[2,*], Badr Almutairi[7] and D. Iranian[4]

[1] Department of Sciences and Technology, Institute of Sciences, University Center of Barika M'doukal Road, 05001 Barika, Algeria
[2] Department of Cybersecurity, College of Computer, Qassim University, Saudi Arabia
[3] Artificial Intelligence Research Centre for Islam and Sustainability (AIRIS), Universiti Sultan Zainal Abidin, Gongbadak, Terengganu 21300, Malaysia
[4] Department of Mathematical Sciences, Saveetha School of Engineering, SIMATS, Chennai, Tamilnadu 602105, India
[5] Department of Mechanical Engineering, Universitas Muhammadiyah Tasikmalaya, Tasikmalaya 46196, Indonesia
[6] College of Applied and Health Sciences, A'Sharqiyah University, Ibra 400, Sultanate of Oman
[7] College of Computer and Information Sciences, Majmaah University, Almajmaah, Saudi Arabia

* **Correspondence:** Email: almaymuni@qu.edu.sa; acengs@umtas.ac.id.

Abstract: In this paper, we propose a new five-dimensional system that is capable of producing multistability and hyperchaos with three positive Lyapunov exponents (LEs) for specific parameter settings. The proposed system was derived by making an extension of Dong's chaotic system with changes that increase its dimension, complexity, and applicability. Using numerical simulations, we confirmed that the model produces hyperchaos with three positive LEs depending on parameter values, which means that its dynamics expands in three directions of the phase space. Regions of periodicity, chaos, hyperchaos with two positive LEs, and hyperchaos with three positive LEs were identified by LE spectra and verified using phase diagrams. The ability of the system to generate coexisting attractors is also shown, where the system demonstrates various behaviors for various initial conditions at fixed parameters. Furthermore, offset boosting control is presented to show that the attractors can be shifted without altering the internal dynamics of the system. Moreover, a topological complexity optimization framework is proposed to maximize the Kaplan–Yorke dimension (KYD) using Particle Swarm Optimization (PSO) and Differential Evolution (DE), followed by the 0–1 test and Approximate Entropy calculation. With its multistability, properties, hyperchaos with three positive LEs, controllable offset boosting, and optimized complexity, the novel model has excellent potential for practical applications.

Keywords: hyperchaos; Lyapunov exponent; multistability; coexisting attractors; offset boosting; optimization method
Mathematics Subject Classification: 37D45, 37M25, 37N35, 93C10

1. Introduction

Over the last years, chaotic systems have been explored in depth to understand their nonlinear dynamics and determine their potential applications in fields of science and engineering [1,2]. The chaos is a kind of deterministic behavior that is unpredictable and is found only in nonlinear systems, which has an extreme sensitivity to initial conditions. Its characteristics have turned chaotic systems into a number of great practical applications such as secure communication [3,4], image and video encryption [5,6], random number generation [7,8], and the modeling of natural phenomena [9–11].

In 1963, the finding of the Lorenz system [12] was a significant moment in the history of chaos theory and it enabled the world of science to embark on extensive studies of the nonlinear dynamics field. From that time on, several three-dimensional (3D) chaotic systems have been unveiled, such as the Rössler system [13], Chen system [14], and Lü system [15], all having different dynamical features. However, it is worth noting that although 3D systems are capable of generating chaos, their complexity is limited since they have only one positive Lyapunov exponent (LE).

To bypass such flaws and obtain more complex dynamical characteristics, researchers have increased the dimensionality of 3D chaotic systems to develop hyperchaotic systems, which are characterized by having no less than two positive LEs. Hyperchaos demonstrates the simultaneous divergence in several directions in phase space, which not only makes it more difficult to predict but also enhances its potential for exploiting in the engineering sector, such as in advanced encryption schemes [16,17]. Although these developments have been achieved, most hyperchaotic systems are four-dimensional (4D) and limited to two positive LEs [18,19]. Producing systems with three or more positive LEs is challenging but important since it enables even greater unpredictability and complexity in the generated signals. They can generate hyperchaos with behavior that expand in more than two directions of phase space [20,21].

One of the contributions on the design of hyperchaotic systems with multiple positive LEs is Dong's research work [22] on designing a novel autonomous 4D hyperchaotic system with double-wing hidden attractors based on its original 3D chaotic system [23]. Nevertheless, this 4D generalization, as well as most of its similarities in the literature, remains capable of producing only two positive LEs. In this paper, we attempt to overcome these limitations through the construction of a new five-dimensional (5D) hyperchaotic system with three positive LEs. Our construction is in the form of Dong's 4D hyperchaotic system but with the incorporation of some key modifications:

- A linear feedback controller is integrated to offer improved control of the system's dynamics.
- A fifth state variable is introduced, which increases the dimension and complexity of the system.
- The parameter set is thoughtfully tuned such that some parameter values are changed and a new parameter is added to offer more flexibility and control over system behavior.

Through these modifications, the proposed 5D system not only produces hyperchaotic attractors with three positive LEs but is also multistable, under which different attractors coexist for the same parameter values but different initial conditions. This feature is greatly desirable in practical applications since it holds the benefit of having increased complexity and unpredictability in signal generation.

To analyze the dynamic behavior of the proposed system, classical nonlinear dynamics tools such as phase portraits, LE spectra, and Kaplan - Yorke dimension (KYD) are employed. numerical simulations show transitions between periodicity, chaos, hyperchaos with two positive LEs, and hyperchaos with three positive LEs when parameters are varied. The multistability phenomenon is investigated in detail by simulating the system with different initial conditions. We observe that the system can produce coexisting periodic attractors and coexisting chaotic attractors, which demonstrates rich dynamics. We also apply an offset boosting control strategy for the 5D system. Offset boosting is an operation enabling the attractor to shift on a chosen axis without modifying the internal dynamics of the system. The procedure is important for applications like secure communication, in which amplitude and position control of the chaotic signal is needed for enhancing the security of the secret message.

The major contributions and novelties of this work can be summarized as follows:

- A novel five-dimensional hyperchaotic system is proposed by extending the original 3D Dong chaotic system through the introduction of a linear feedback controller and an additional state variable, enabling the generation of hyperchaos with three positive LEs.
- The proposed system demonstrates rich nonlinear behaviors, including periodicity, chaos, hyperchaos, multistability, coexisting attractors, and offset boosting control, which significantly enhance the dynamical complexity and unpredictability of the system.
- Advanced complexity validation and optimization methods, including two-dimensional Lyapunov heatmaps, 0–1 chaos test, approximate entropy analysis, and metaheuristic optimization (DE and PSO), are employed to maximize the KYD and confirm the suitability of the proposed system for secure communication, cryptography, and pseudo-random number generation applications.

The remaining part of this paper is organized as follows: In Section 2, we introduce the mathematical formulation of the proposed 5D hyperchaotic system. In Section 3, we address the influence of system parameters on its dynamics, i.e., periodic-chaotic-hyperchaotic transitions. In Section 4, we explore the multistability phenomenon through coexisting attractors analysis. In Section 5, we introduce offset boosting control and its influence on the chaotic dynamics of the system. In Section 6, we provide the optimization of topological complexity via metaheuristic algorithms. In Section 7, we present the 0-1 test and approximate entropy of the hyperchaotic system. Finally, in Section 8, we conclude the paper and provide options for future research.

2. Construction of the new 5D hyperchaotic system

In 2022, Dong [23] proposed a new 3D chaotic system capable of generating two-wing hidden attractors. They provide a detailed analysis of the system's dynamics under varying parameters and initial conditions. The mathematical model of this system is described by the following set of differential equations:

$$\begin{cases} \dot{x} = a(y-x) + kxz, \\ \dot{y} = -cy - xz, \\ \dot{z} = -b + xy. \end{cases} \tag{1}$$

The constants a, b, c, and k are the major parameters of the system. When these parameters are set to $(a, b, c, k) = (10, 100, 11.2, -0.2)$, the system shows a hidden chaotic attractor with one positive LE. Its dynamic behavior, periodic orbits, and circuit implementation have been studied in detail in [23].

In the same year, Dong published another paper [22] in which the original 3D chaotic system (1) was extended to a 4D system by introducing a linear state feedback controller into the first equation of system (1). This modification ensured that the minimal dimension required to generate hyperchaos was achieved. As a result, the system exhibits two positive LEs, along with one zero and one negative LE, leading to the following 4D autonomous hyperchaotic system:

$$\begin{cases} \dot{x} = a(y-x) + kxz + w, \\ \dot{y} = -cy - xz, \\ \dot{z} = -b + xy, \\ \dot{w} = -my. \end{cases} \tag{2}$$

When the parameters are set to $(a, b, c, k, m) = (10, 100, 2.7, -0.2, 1)$ and the initial conditions are $(x_0, y_0, z_0, w_0) = (1, 1, 1, 1)$, system (2) generates hidden hyperchaotic attractors with two positive LEs and shows more complex behavior compared to the original 3D system (1). Its dynamic behavior, periodic orbits, and circuit implementation have been studied in detail in [22].

In this paper, we introduce a new 5D hyperchaotic system with improved features by modifying Dong's 4D system (2). A linear feedback controller is added to the fourth state of system (1). We also adjust the parameter values for our system (3) by modifying the values of a and b, setting the parameters c and m to 1 and removing them from the model while introducing a new parameter d in the fifth equation of the system. The resulting model is given as follows:

$$\begin{cases} \dot{x} = a(y-x) + kxz + w, \\ \dot{y} = -y - xz, \\ \dot{z} = -b + xy, \\ \dot{w} = -y + u, \\ \dot{u} = -y - dw. \end{cases} \tag{3}$$

When the parameters are set to $(a, b, d, k) = (8, 50, 0.2, -0.2)$ and the initial conditions are $(x_0, y_0, z_0, w_0, u_0) = (1, 1, 1, 1, 0)$, system (3) produces hyperchaotic attractors with three positive LEs and displays more complex behavior compared to the original 3D system (1) and the extended 4D system (4). Different phase plots of the attractors of system (3) are shown in Figure 1. For $T = 1 \times 10^4$, with initial conditions $(x_0, y_0, z_0, w_0, u_0) = (1, 1, 1, 1, 0)$ and parameters $(a, b, d, k) = (8, 50, 0.2, -0.2)$, the LEs (LEs) for the new 5D system (3) are calculated using the Wolf's Algorithm [24] as follows:

$$L_1 = 0.7517,\ L_2 = 0.0669,\ L_3 = 0.0365,\ L_4 = 0,\ L_5 = -9.5081. \tag{4}$$

Using the LEs in Eq (4), the KYD for system (3) is computed as:

$$D_{KY} = 4 + \frac{L_1 + L_2 + L_3 + L_4}{|L_5|} = 4.0899. \tag{5}$$

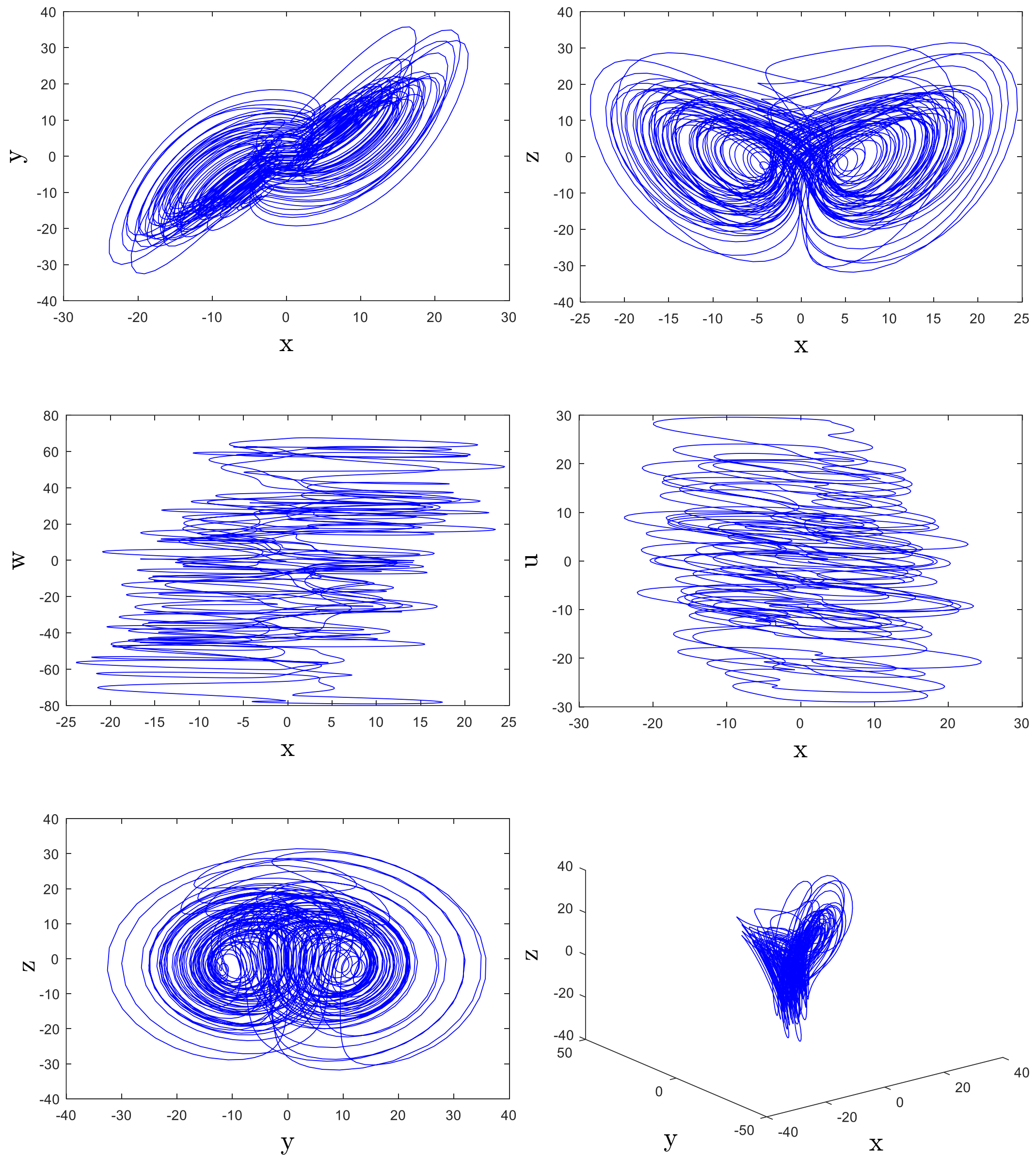

Figure 1. Hyperchaotic attractors of the proposed system (3).

Table 1 compares the signs of the LEs and the KYD of the proposed 5D system (3) with the original 3D system [23], the 4D system [22], and eight other reported 5D systems.

Table 1. Comparison between the systems in Dong [23], Dong [22], the proposed 5D system (3), and other 5D systems.

System	Dimension	L1	L2	L3	L4	L5	KYD
Dong [23]	**3**	+	**0**	**-**			**2.0267**
Dong [22]	**4**	+	+	**0**	**-**		**3.0696**
Our system(3)	**5**	+	+	+	**0**	**-**	**4.0899**
Yu [25]	**5**	+	**0**	**-**	**-**	**-**	**3.1667**
Dong [26]	**5**	+	**0**	**-**	**-**	**-**	**2.6065**
Zhuang [27]	**5**	+	**0**	**-**	**-**	**-**	**3.6525**
Johansyah [28]	**5**	+	**0**	**-**	**-**	**-**	**2.2518**
Sagban [29]	**5**	+	+	**0**	**-**	**-**	**4.0849**
Xiu [30]	**5**	+	+	**0**	**-**	**-**	**3.1220**
Khattar [31]	**5**	+	+	**0**	**-**	**-**	**3.0575**
Niu [32]	**5**	+	+	**0**	**-**	**-**	**4.0502**

In Table 1, the proposed system exhibits three positive LEs, indicating that its trajectories expand along three independent directions in phase space, thus confirming strong hyperchaotic behavior with high dynamical complexity. In contrast, the 4D system of Dong [22] has only two positive LEs, while the 3D system [23] possesses a single positive exponent, reflecting lower-complexity chaotic dynamics. Furthermore, compared with some other 5D systems, which generally exhibit at most two positive exponents, the proposed model stands out by maintaining three strictly positive LEs. In addition, the KYD of the proposed system (4.0899) is the highest among the compared systems, indicating a higher fractal dimensionality and a richer attractor structure. These results demonstrate that the proposed system not only increases the dimensionality but also significantly enhances the complexity and unpredictability of the dynamics, making it particularly suitable for applications requiring highly complex chaotic behavior.

To further characterize the global dynamics of system (3), we investigate its dissipativity. The divergence of the vector field is given by

$$V=\frac{\partial x}{\partial \dot{x}}+\frac{\partial y}{\partial \dot{y}}+\frac{\partial z}{\partial \dot{z}}+\frac{\partial w}{\partial \dot{w}}+\frac{\partial u}{\partial \dot{u}}=-9-0.2z. \tag{6}$$

Thus, the dissipative nature of the trajectories in system (3) is demonstrated by the time-averaged value of ($v(t)$ =−9−0.2$z(t)$). The new hyperchaotic system (3) is considered dissipative if the time-averaged value of v(t) is negative. Following the methodology in [29], the average value of v(t) is defined as:

$$\lim_{t\to\infty}\frac{1}{T}\int_0^T \mathrm{v}(t)dt=\lim_{t\to\infty}\frac{1}{T}\int_0^T(-9-0.2z(t))dt. \tag{7}$$

To assess the long-term behavior, we compute the time-averaged value of $v(t)$ over a sufficiently large interval T=10^5 (for chaotic systems, a simulation time of T = 10^5 is highly sufficient to guarantee numerical convergence and an accurate characterization of the asymptotic dynamical behavior). Our numerical simulation yields a stable average value of -8.9988, as shown in Figure 2. The negative value ensures that the system's trajectories are confined to a specific region and asymptotically converge toward a strange attractor of fractional dimension.

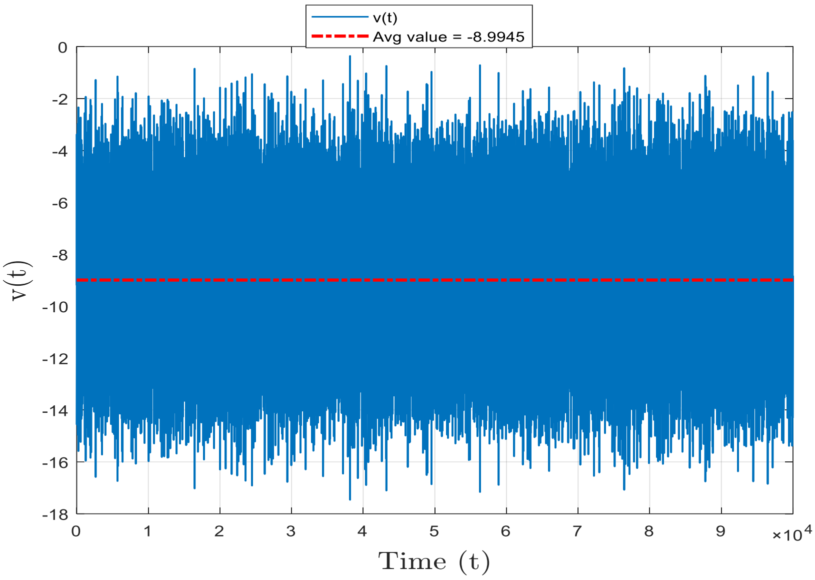

Figure 2. Time evolution of v(t) with an average value of -8.9988.

3. Influence of parameters on system behavior

In this section, we analyze how the system's behavior evolves with parameter variations, identifying regions of hyperchaos (three and two positive LEs), chaos (one positive LE), and periodic behavior. The parameter ranges are selected based on a preliminary exploration of the parameter space, as the model is highly sensitive to parameter changes. Outside these intervals, the system tends to diverge or exhibits similar dynamics temporarily before diverging. The chosen ranges ensure bounded trajectories while preserving strong nonlinear sensitivity, enabling the system to exhibit rich and complex dynamics.

In addition, we extend this analysis by studying two-dimensional LE heatmaps in different parameter planes to provide a more comprehensive view of the system's global dynamical behavior and robustness under parameter variations. The dynamics of system (3) with different parameter values can be seen in Table 2.

Table 2. LEs, KYD, and dynamics of system (3) with different parameter values.

	Interval	Selected value	L1	L2	L3	L4	L5	KYD	Dynamics
a	[0, 2]	0.5	**0**	-0.081	-0.391	-0.499	-0.510	0	Periodic
	[2, 5.4]	5.2	0.170	**0**	-0.127	-0.208	-5.872	3.207	Chaos
	[5.4, 8]	7	0.771	0.080	0.032	**0**	-8.545	4.103	Hyperchaos
b	[0, 6.9]	4	**0**	-0.078	-0.099	-0.251	-7.484	0	Periodic
	[6.9, 8.5]	7.2	0.012	**0**	-0.093	-0.207	-7.589	2.129	Chaos
	[8.5, 30]	20	0.132	0.048	**0**	-0.050	-7.873	4.016	Hyperchaos
	[30, 50]	48	0.833	0.073	0.044	**0**	-8.597	4.111	Hyperchaos
d	[0.01, 0.08]	0.07	0.118	**0**	-0.193	-0.309	-7.499	2.611	Chaos
	[0.08, 0.12]	0.09	0.170	0.039	**0**	-0.283	-7.590	3.739	Hyperchaos
	[0.12, 0.3]	0.14	0.808	0.095	0.008	**0**	-8.538	4.107	Hyperchaos
k	[-3, -1]	-1.5	0.006	**0**	-0.226	-0.485	-6.934	2.066	Chaos
	[-1, -0.4]	-0.8	0.076	0.021	**0**	-0.264	-7.015	3.367	Hyperchaos
	[-0.4, 0]	-0.1	0.789	0.093	0.012	**0**	-8.680	4.103	Hyperchaos

3.1. Effect of varying parameter a

To study how changing the parameter a affect the dynamics of system (3), we fix the other parameters as (b, d, k) = (50, 0.2, −0.2) and vary a from 0 to 8. For these values, we plot the LEs (LEs) diagram shown in Figure 3(a) and the bifurcation diagram shown in Figure 3(b). For clarity, we display only L_1, L_2, L_3, and L_4 since L_5 is always negative. From Figure 3(a), we can identify regions with different behaviors and plot the corresponding attractors. When a varies between 0 and 2, Figure 3(a) shows one zero LE and four negative LEs, which indicates that system (3) has periodic behavior in this range of a. This is confirmed by the attractor plotted in Figure 3(c) for a = 0.5, with its corresponding LEs and KYD listed in Table 2.

When a varies between 2 and 5.4, system (3) has one positive LE, meaning it shifts to chaotic behavior, as illustrated by the attractor in Figure 3(d) for a = 5.2, with its LEs and KYD also shown in Table 2. Finally, when a varies from 5.4 to 8, Figure 3(a) shows three positive LEs. This means that, in this range of a, system (3) exhibits complex hyperchaotic behavior with dynamics expanding in three different directions of phase space. The corresponding attractor is shown in Figure 3(e) for a = 7, with its LEs and KYD provided in Table 2.

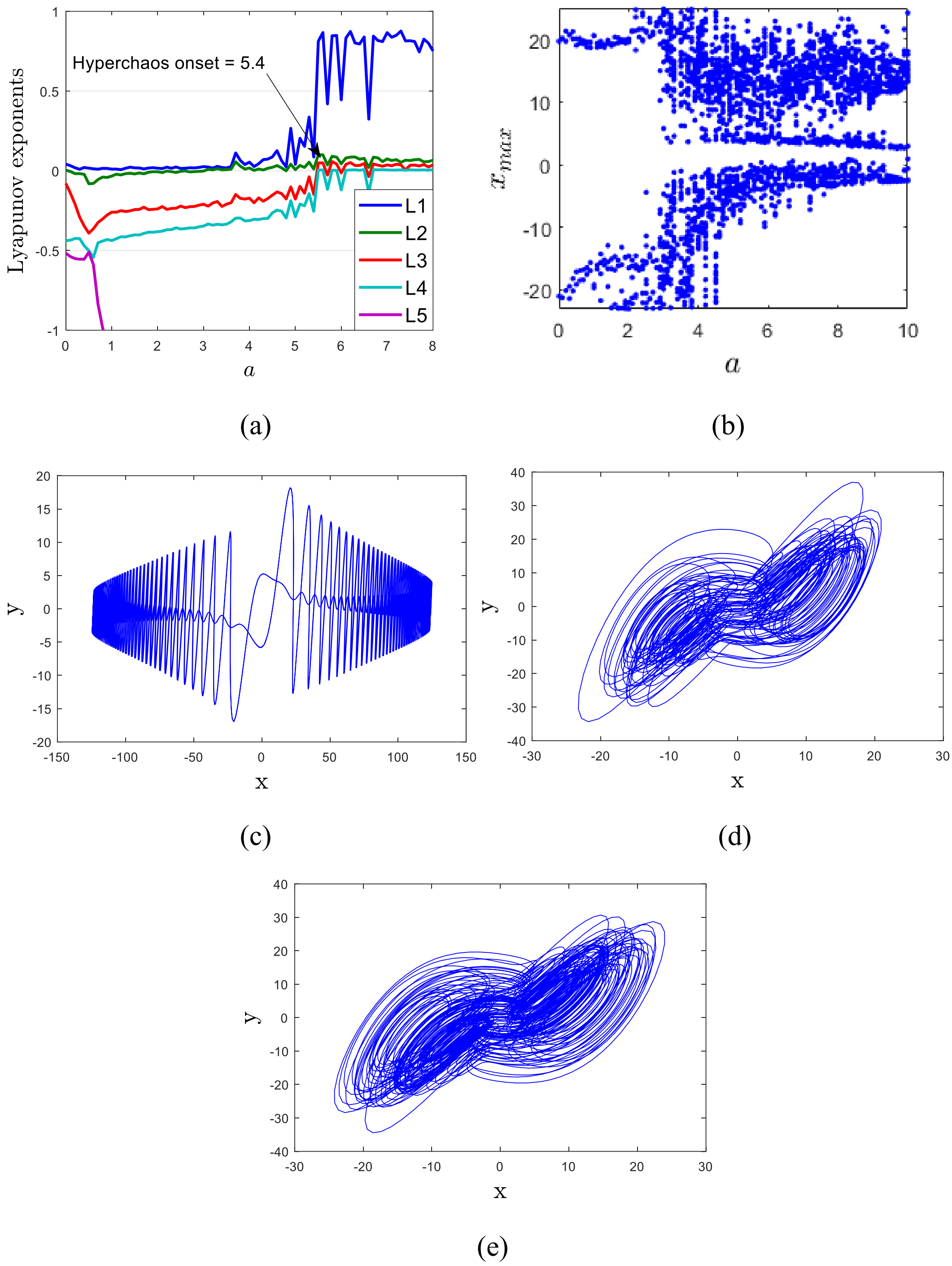

Figure 3. (a) LEs and (b) bifurcation diagram for $0 < a < 8$, (c) x-y periodic attractor for a=0.5, (d) x-y chaotic attractor for a=5.2, and (e) x-y hyperchaotic attractor with three LEs for a=7.

3.2. Effect of varying parameter b

To study how changing parameter b affects the dynamics of system (3), we fix the other parameters as $(a, d, k) = (8, 0.2, -0.2)$ and vary b from 0 to 50. For these values, we plot the LEs (LEs) diagram shown in Figure 4(a) and the bifurcation diagram shown in Figure 4(b). For clarity, we display only L_1, L_2, L_3, and L_4 since L_5 is always negative. From Figure 4(a), we can identify regions with different behaviors: Periodic, chaos, hyperchaos with two LEs, and hyperchaos with three LEs.

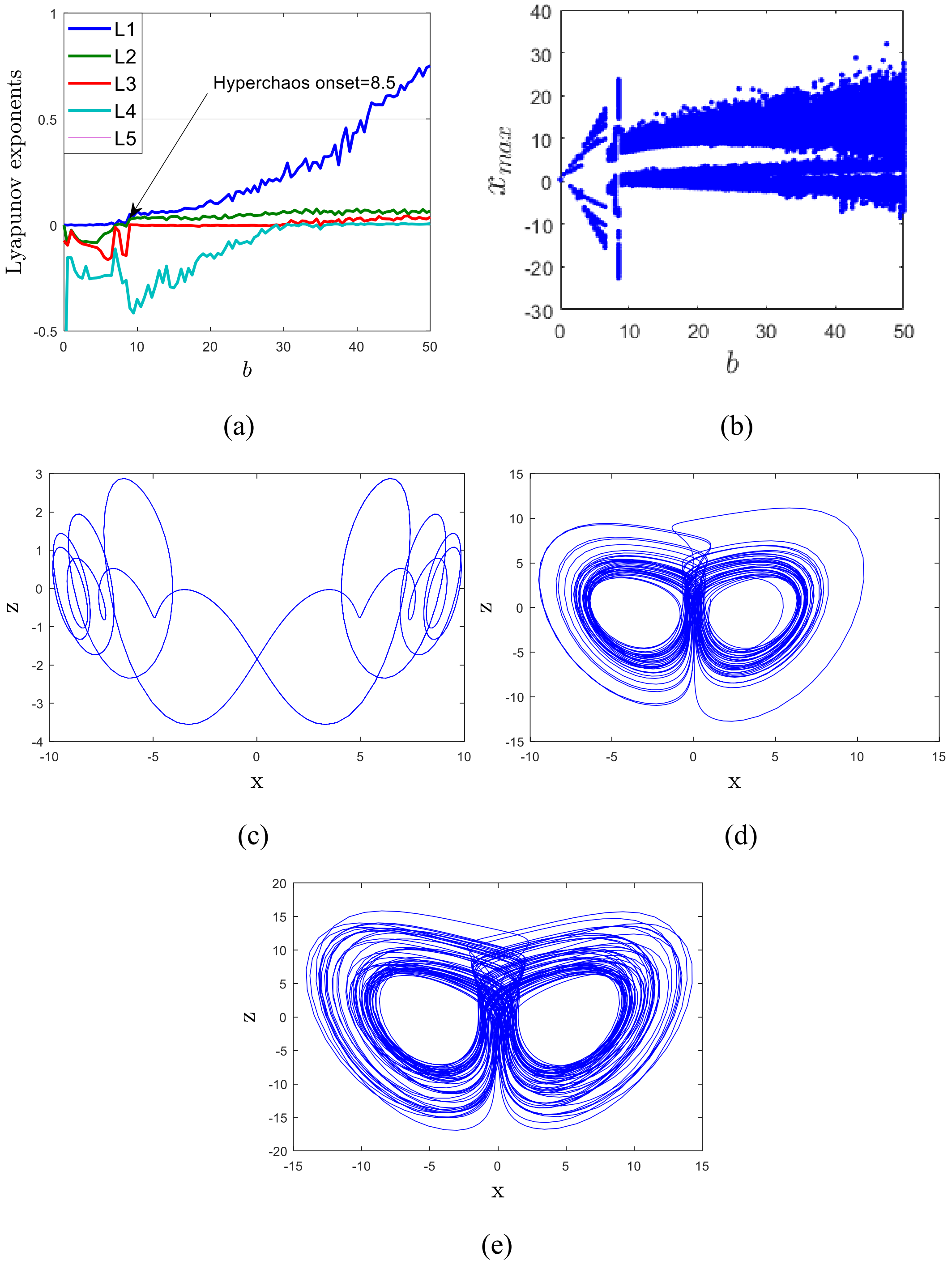

Figure 4. (a) LEs and (b) bifurcation diagram for 0<b<50, (c) x-z periodic attractor for b=4, (d) x-z chaotic attractor for b=8, (e) x-z hyperchaotic attractor with two LEs for b=20, and (f) x-z hyperchaotic attractor with three LEs for b=48.

When b varies between 0 and 7, Figure 4(a) shows one zero LE and four negative LEs, indicating that system (3) has periodic behavior in this range of b. This is confirmed by the attractor in Figure 4(c) for b = 4, with its corresponding LEs and KYD listed in Table 2. As b increases to the range of 7 to 8.5, system (3) shows one positive LE, which means it transitions to chaotic behavior. This is illustrated by the attractor in Figure 4(d) for $b = 8$, with its LEs and KYD shown in Table 2.

For b values between 8.5 and 30, Figure 4(a) displays two positive LEs, which means the system exhibits more complex behavior, with its dynamics expanding in two different directions of phase space. The attractor for $b = 20$ is shown in Figure 4(e), with the LEs and KYD listed in Table 2. Finally, when b varies from 30 to 50, Figure 4(a) shows three positive LEs. In this range, system (3) exhibits highly complex hyperchaotic behavior, with its dynamics expanding in three directions of phase space. The corresponding attractor for $b = 48$ is shown in Figure 4(f), with its LEs and KYD provided in Table 2.

3.3. Effect of varying parameter d

To study how changing parameter d affects the dynamics of system (3), we fix the other parameters as $(a, b, k) = (8, 50, -0.2)$ and vary d from 0.01 to 0.3. For these values, we plot the LEs (LEs) diagram shown in Figure 5(a) and the bifurcation diagram shown in Figure 5(b). For clarity, we display only L_1, L_2, L_3, and L_4 since L_5 is always negative. From Figure 5(a), we can identify regions with different behaviors: chaos, hyperchaos with two LEs, and hyperchaos with three LEs.

As d increases from 0.01 to 0.08, system (3) shows one positive LE, indicating chaotic behavior. This is illustrated by the attractor in Figure 5(c) for $d = 0.07$. The corresponding LEs and KYD are listed in Table 2. When d is between 0.08 and 0.12, Figure 5(a) shows two positive LEs, meaning the system becomes more complex, with dynamics expanding in two directions of phase space. The attractor for $d = 0.09$ is shown in Figure 5(d), with its LEs and KYD given in Table 2. Finally, as d increases from 0.12 to 0.3, Figure 5(a) displays three positive LEs. In this range, system (3) exhibits highly complex hyperchaotic behavior with dynamics expanding in three different directions of phase space. The attractor for $d = 0.14$ is shown in Figure 5(e), with its LEs and KYD presented in Table 2.

3.4. Effect of varying parameter k

To study how changing parameter k affects the dynamics of system (3), we fix the other parameters as $(a, \mathrm{b}, \mathrm{d}) = (8, 50, 0.2)$ and vary k from -3 to 0. For these values, we plot the LEs (LEs) diagram shown in Figure 6(a) and the bifurcation diagram shown in Figure 6(b). For clarity, we display only L_1, L_2, L_3, and L_4 since L_5 is always negative. From Figure 6(a), we can identify regions with different behaviors: chaos, hyperchaos with two LEs, and hyperchaos with three LEs.

As parameter k increases from -3 to -1, system (3) has one positive LE, which indicates chaotic behavior. This is shown by the attractor in Figure 6(c) for $k = -1.5$. The corresponding LEs and KYD are provided in Table 2. When k is in the range -1 to -0.4, Figure 6(a) shows two positive LEs, meaning the system becomes more complex with dynamics expanding in two directions of phase space. The attractor for $k = -0.8$ is displayed in Figure 6(d), and its LEs and KYD are listed in Table 2. Finally, as parameter k varies from -0.4 to 0, Figure 6(a) shows three positive LEs. In this range, system (3) exhibits highly complex hyperchaotic behavior with dynamics expanding in three different directions of phase space. The attractor for $k = -0.1$ is shown in Figure 6(e), with its LEs and KYD presented in Table 2.

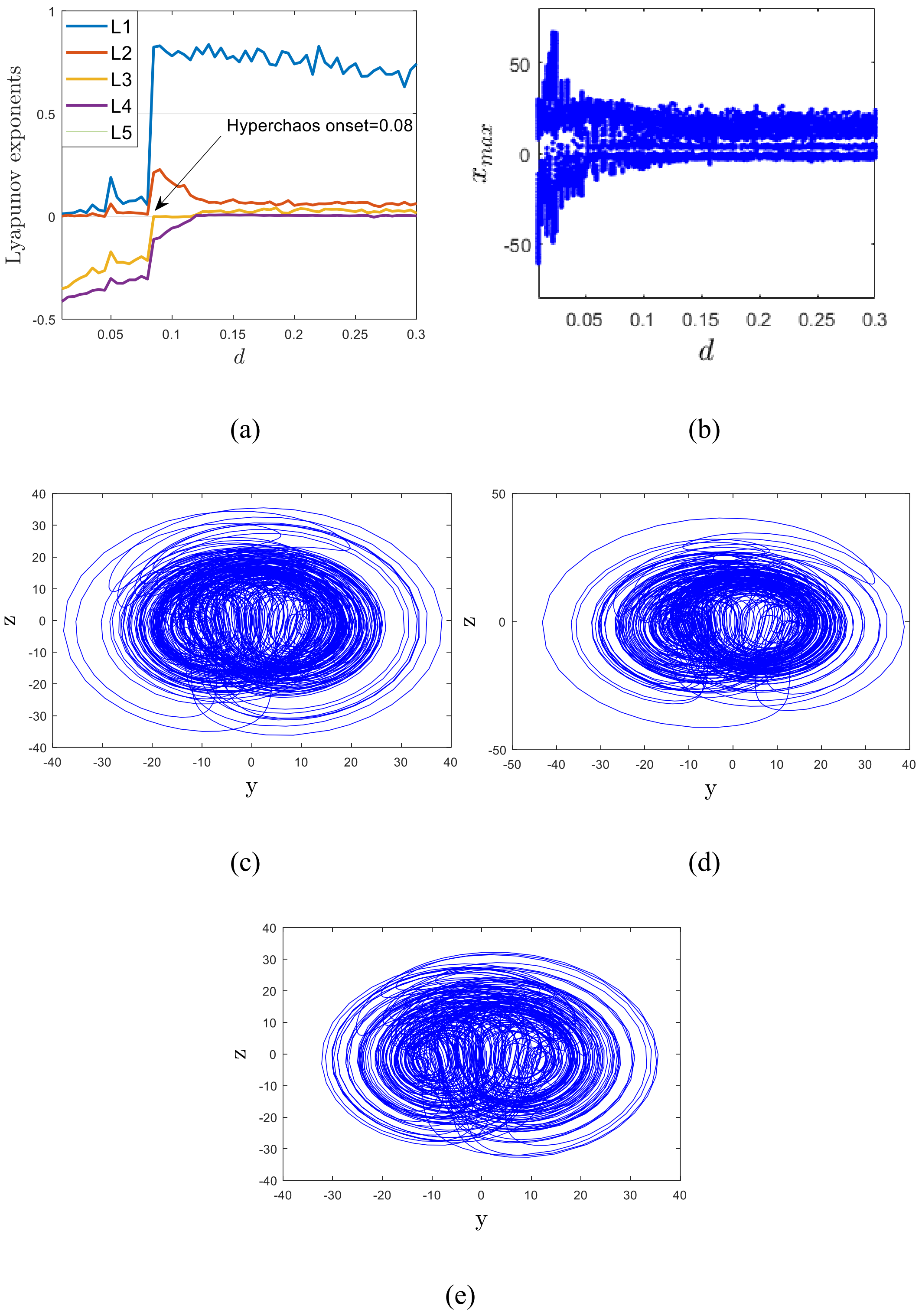

Figure 5. (a) LEs and (b) bifurcation diagram for $0.01 < d < 0.3$, (c) y-z chaotic attractor for d=0.07, (d) y-z hyperchaotic attractor with two LEs for d=0.09, and (e) y-z hyperchaotic attractor with three LEs for b=0.14.

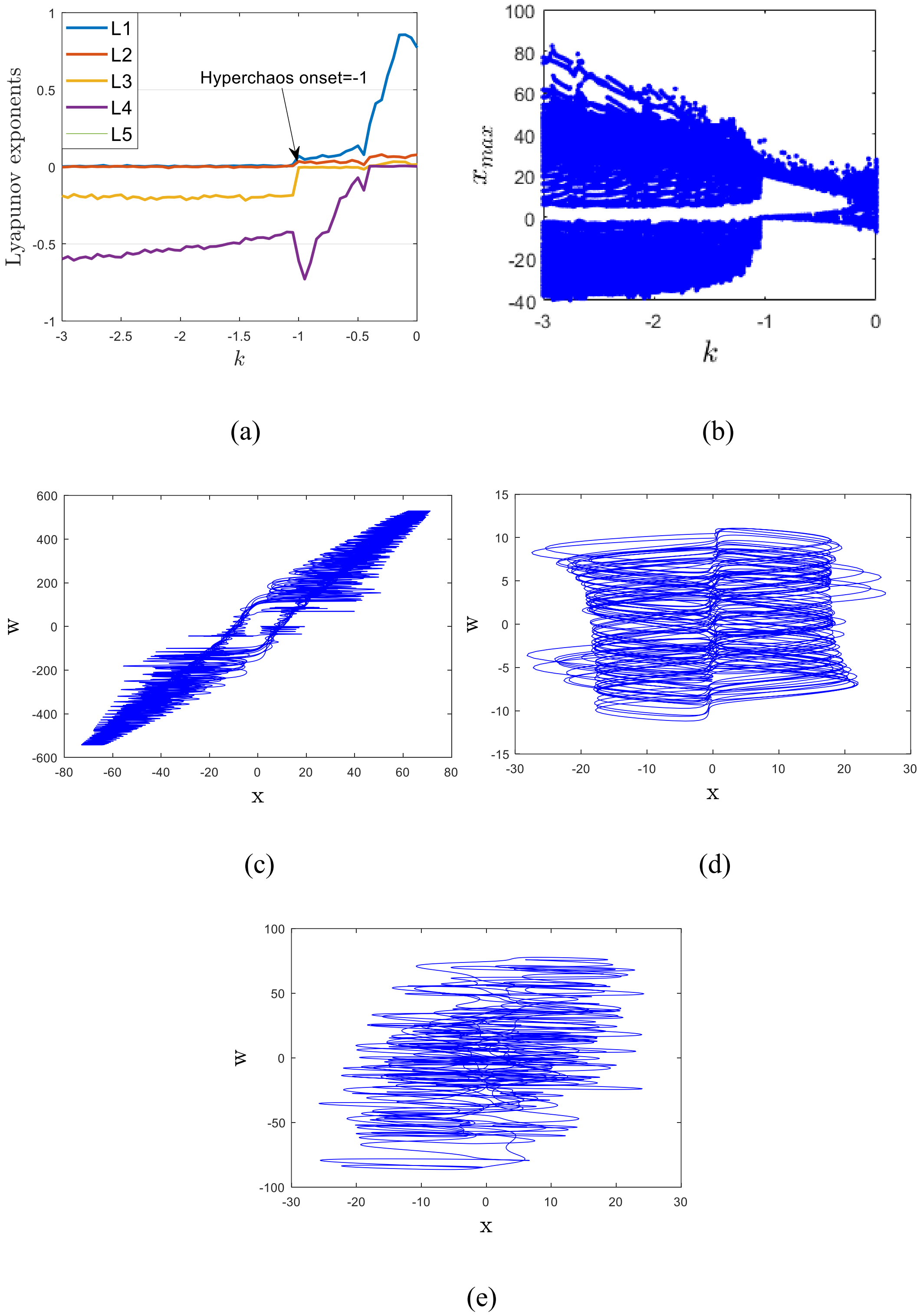

Figure 6. (a) LEs and (b) bifurcation diagram for -3 < k < 0, (c) x-w chaotic attractor for k=-1.5, (d) x-w hyperchaotic attractor with two LEs for k=-0.8, and (e) x-w hyperchaotic attractor with three LEs for k=-0.1.

3.5. Two-dimensional LE heatmaps analysis

To demonstrate the dynamical robustness of the proposed 5D system, two-dimensional regime heatmaps are constructed in the (a, b), (a, d), (a, k), (b, d), (b, k), and (d, k) parameter planes, as shown in Figures 7(a)−(f). Contrary to the assumption that high-order hyperchaos exists only as isolated "islands", these maps reveal broad, continuous, and well-connected regions of triple-positive LEs indicated in amber, alongside hyperchaotic regions with two positive exponents in deep orange. The presence of these orange zones surrounding the amber regions indicates a smooth transition between levels of hyperchaotic behavior rather than a loss of complexity or divergence. Such parametric continuity is a fundamental topological property that ensures the high-order hyperchaotic state is robust rather than a fragile numerical artifact. This stability is critical for hardware implementations in physical circuits or embedded systems, where component tolerances inevitably lead to slight variations in parameters. The broadness of the amber regions ensures that the system maintains high-complexity hyperchaotic behavior despite these variations, providing a reliable, entropy-rich source for practical engineering applications such as random number generation and secure communications.

4. Influence of initial conditions on system behavior

To study the phenomenon of multistability, we plot the basins of attraction and attractors of system (3) in this section by selecting different initial points while keeping the same parameter values.

- For the parameter values (a, b, d, k) = (8, 1, 0.2, -0.2), we compute and visualize the basins of attraction of system (3) in the three-dimensional (y_0, z_0, u_0) space, with $y_0 \in [0, 1]$, $z_0 \in [0,1]$, and $u_0 \in [0,1]$. The corresponding results are presented in Figure 8(a). We observe that, for these parameter values, system (3) exhibits multistability in the form of two coexisting periodic attractors. Figure 8(b) illustrates the basin of attraction associated with the first periodic regime, showing the set of initial conditions that converge to this attractor. Similarly, Figure 8(c) depicts the basin of attraction of the second periodic regime, highlighting the set of initial conditions leading to the second coexisting attractor. Representative phase portraits of the two periodic attractors are shown in Figures 8(d)−(f). Based on the basin structure, we select two initial conditions: X_{01} = (1,0,0,1,0) and X_{02} = (1,1,1,1,0). The trajectories plotted in blue correspond to X_{01}, while those in red correspond to X_{02}.
- For (a, b, d, k) = (8, 7, 0.2, -0.2), the basins of attraction of system (3) are computed in the (y_0, z_0, u_0) space with (y_0, z_0, u_0)$\in$ [0,1], as shown in Figure 9(a). The system exhibits multistability with two coexisting chaotic attractors. Figures 9(b),(c) present the corresponding basins, identifying initial conditions leading to each chaotic regime. Representative phase portraits are shown in Figures 9(d)−(f). Based on the basin structure, two initial conditions are selected: X_{01} = (1,0,0,1,0) and X_{02} = (1,1,1,1,1); trajectories in blue correspond to X_{01}, and those in red correspond to X_{02}.

These results show that our proposed system not only exhibits hyperchaos with three positive LEs but can also display multistability, which increases the complexity of the model and makes it more suitable for engineering applications.

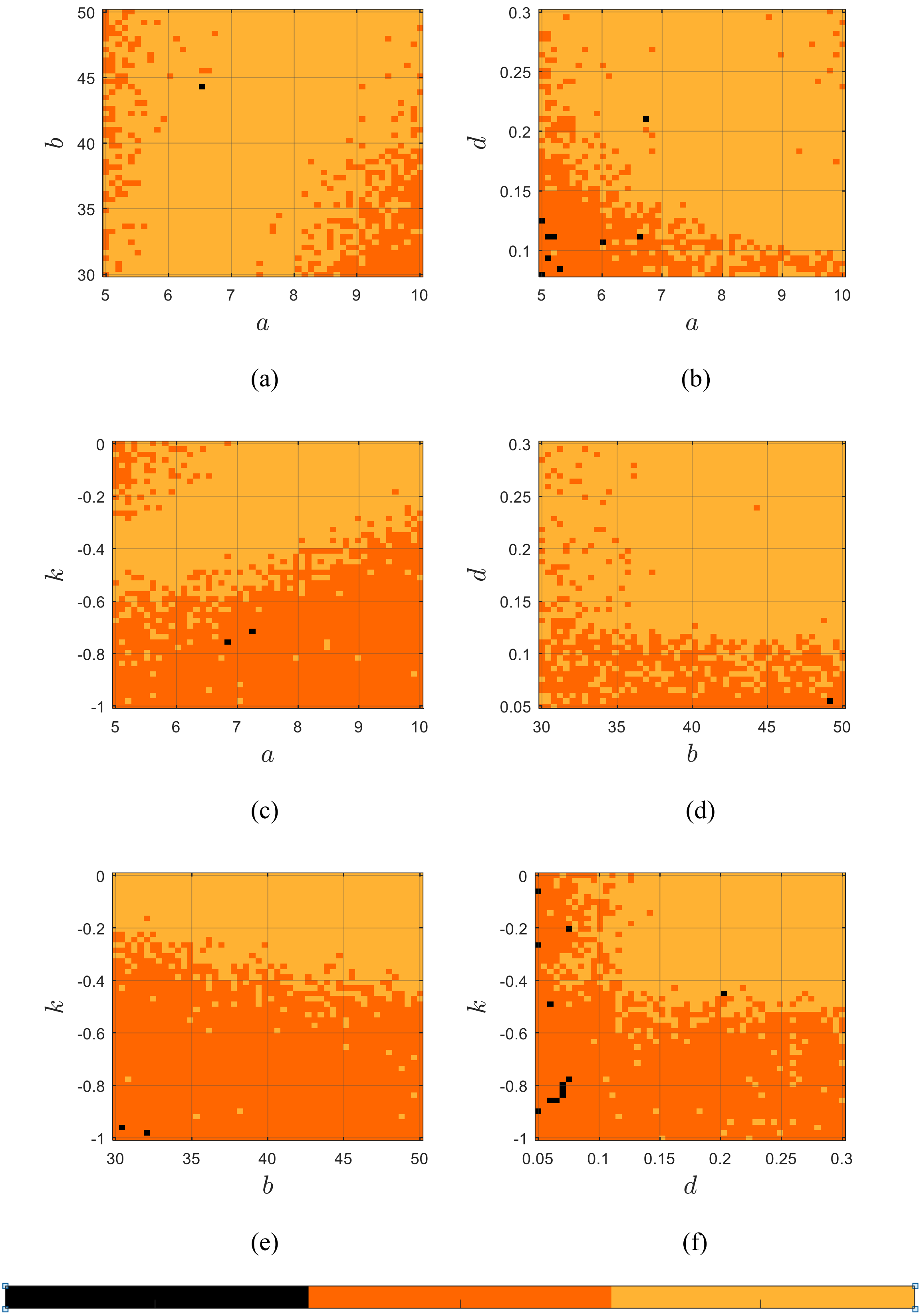

Figure 7. Two-dimensional LE heatmaps illustrating the distribution of hyperchaotic regions in the (a) a-b, (b) a-d, (c) a-k, (d) b-d, (e) b-k, and (f) d-k parameter planes.

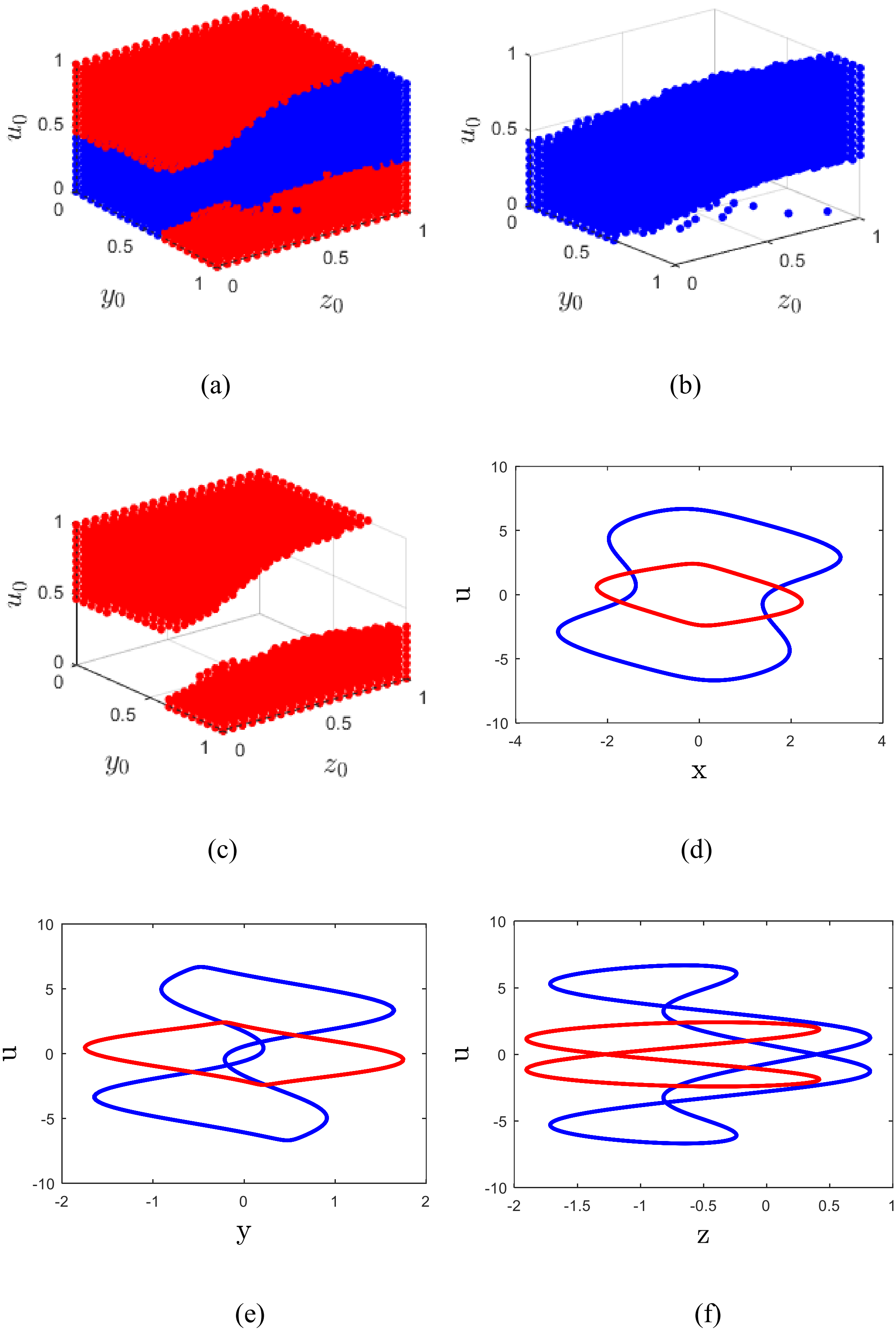

Figure 8. Basins of attraction of system (3) in the (y_0,z_0,u_0) space and phase portraits of two coexisting periodic attractors for (a, b, d, k) = (8, 1, 0.2, −0.2).

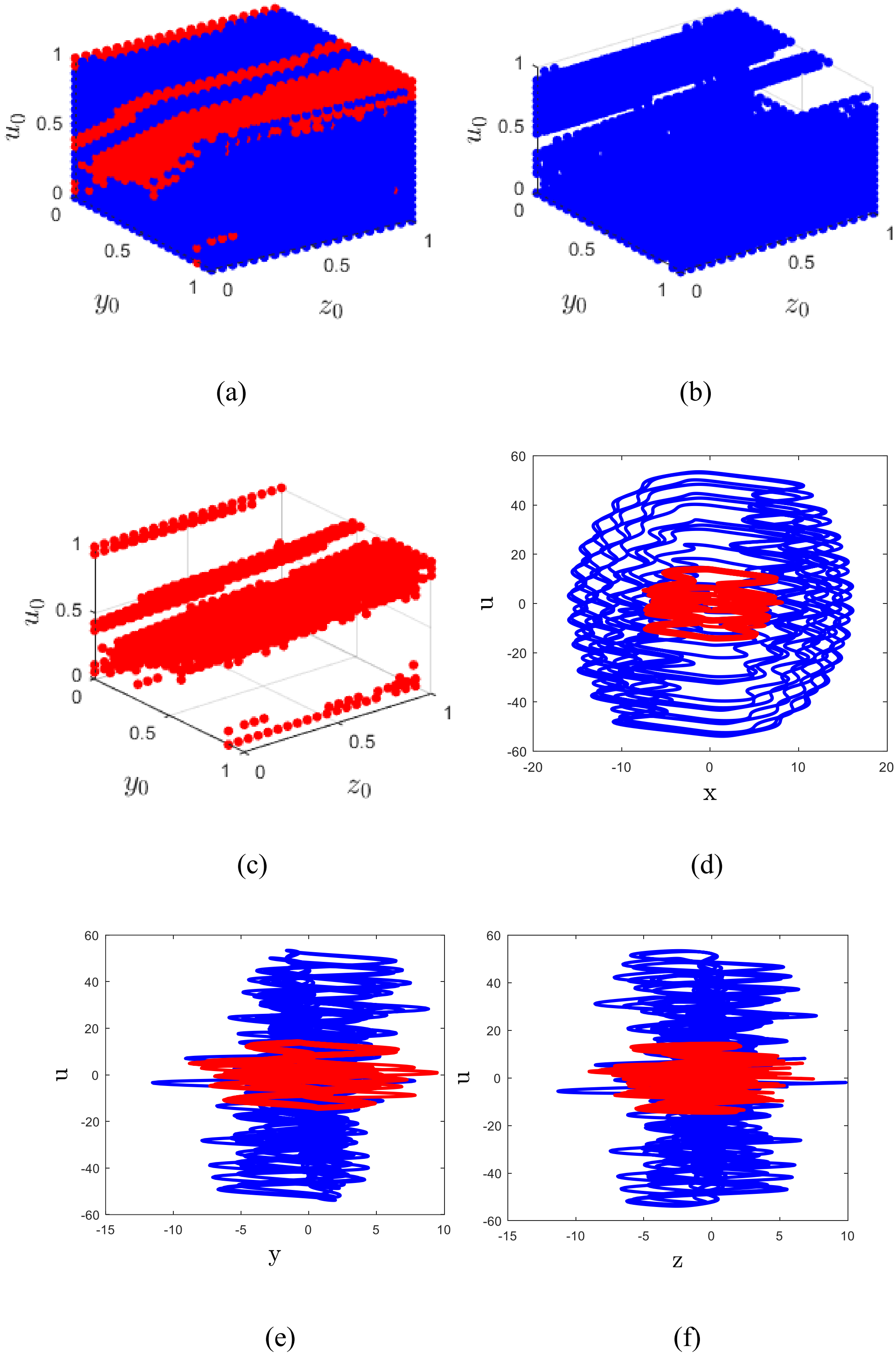

Figure 9. Basins of attraction of system (3) in the (y_0,z_0,u_0) space and phase portraits of two coexisting chaotic attractors for (a, b, d, k) = (8, 7, 0.2, −0.2).

5. Offset boosting control (OBC)

In the proposed 5D system, hyperchaotic behavior with a tunable offset is observed, which has a notable influence on the u variable. By substituting u with $(u + p)$ in the fourth equation of the new system (3), we obtain the following form:

$$\begin{cases} \dot{x} = a(y - x) + kxz + w, \\ \dot{y} = -y - xz, \\ \dot{z} = -b + xy, \\ \dot{w} = -y + (u + p), \\ \dot{u} = -y - dw. \end{cases} \tag{8}$$

OBC is a useful method for adjusting the amplitude of a system by adding a feedback term [33]. While this technique does not change the system's inherent dynamics, it makes it possible to shift the attractor in either direction based on the selected boosting parameter. In our proposed 5D model, the offset boosting mechanism has a strong effect on the position of the hyperchaotic attractor, especially along the u-direction. The magnitude of the state variable u in system (3) can be adjusted, as shown by the w–u phase portrait in Figure 10(a). When parameter p is negative, the attractor shifts in the positive direction, while a positive p shifts it in the negative direction. This feature enables the chaotic signal u to change from a bipolar form to a unipolar one, as illustrated in Figure 10(b). Such behavior demonstrates the strong potential of the proposed system for chaos-based applications.

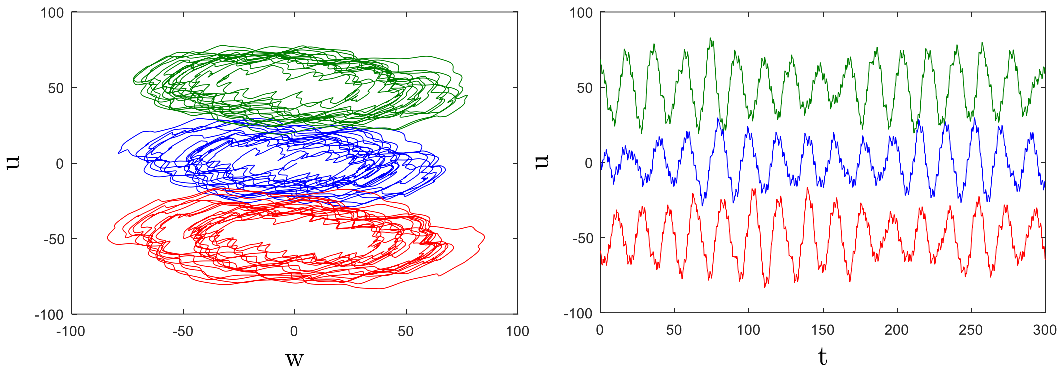

(a) (b)

Figure 10. (a) w-u phase Portrait and (b) u-time series under Offset Control; p=0 (Blue); p=50 (Red), and p=-50 (Green).

6. Optimization of topological complexity via metaheuristic algorithms

In this section, the complexity of the proposed 5D hyperchaotic system is maximized by treating the KYD D_{ky} as an objective function for optimization. Given the high-dimensional nature of the parameter space, two distinct metaheuristic approaches (Particle Swarm Optimization (PSO) and Differential Evolution (DE)) are employed to identify the parameter set $P = [a, b, d, k]$ that yields the highest topological complexity.

6.1. Differential evolution (DE)

DE is a population-based stochastic search algorithm that utilizes vector differences to navigate the search space [34]. In each generation, a mutant vector is created for each target individual by combining the weighted difference of two randomly selected population members with a third member. This mutation process is defined as:

$$V_{i,G+1} = X_{r1,G} + F.\left(X_{r2,G} - X_{r3,G}\right). \tag{9}$$

In the mutation process, $X_{r1,G}$, $X_{r2,G}$, and $X_{r3,G}$ are three distinct vectors randomly selected from the current population such that their indices $r_1 \neq r_2 \neq r_3 \neq i$. G represents the current generation, and F is a mutation constant that scales the differential variation. During the crossover phase, a trial vector $U_{j,i,G+1}$ is generated as follows:

$$U_{i,j,G+1} = \begin{cases} V_{j,i,G+1} \ if \left(rand_j\left(0,1\right) \leq CR\right) \ or \ \left(j = j_{rand}\right), \\ X_{j,i,G} \ otherwise, \end{cases} \tag{10}$$

where $j = \{1, 2, \ldots, D\}$ represents the parameter dimension (with $D = 4$), $CR \in [0, 1]$ is a crossover coefficient determined by the user, and j_{rand} is a randomly generated index ensuring that at least one parameter is inherited from the mutant vector. To ensure numerical stability and physical consistency, a rounding operator is applied to maintain a precision of three decimal places 10^{-3} for all generated trial vectors. During the selection process, the fitness of the trial vector (defined by the KYD D_{ky}) is evaluated using the Wolf algorithm and the ode45 solver. If the trial vector yields a higher D_{ky} than the target vector $X_{i,G}$, it replaces the target vector in the population for the next generation (G+1); otherwise, the target vector is retained. The DE algorithm iterates until the maximum number of generations is reached, at which point the optimal system parameters and the corresponding D_{ky} are retrieved.

6.2. Particle Swarm optimization (PSO)

PSO is a population-based metaheuristic search strategy inspired by the collective intelligence and social behavior of biological populations, such as bird flocks [34]. In this framework, each potential parameter set is treated as a "particle" *i* that occupies a position x_i in the D-dimensional search space and moves with an adaptable velocity v_i. The trajectory of each particle is governed by its own historical success and the overall experience of the swarm. The velocity update for the j-th dimension of the i-th particle is defined as follows:

$$v_{i,j}\left(t+1\right) = wv_{i,j}\left(t\right) + c_1 r_1\left(pbest_{i,j} - x_{i,j}\left(t\right)\right) + c_2 r_2\left(gbest_j - x_{i,j}\left(t\right)\right), \tag{11}$$

where w is the inertia weight that balances global exploration and local exploitation, while c_1 and c_2 are the cognitive and social acceleration coefficients, respectively. The terms r_1 and r_2 are independent random variables sampled from a uniform distribution U(0, 1). Variable $pbest_i$ represents the best position previously visited by particle i, and gbest represents the best position found by the swarm. Following the velocity update, the new position of the particle is determined as:

$$x_{i,j}\left(t+1\right)=x_{i,j}\left(t\right)+v_{i,j}\left(t+1\right), \tag{12}$$

where j = {1, 2, …. , D} represents the parameter dimension (with D=4). To maintain numerical stability and satisfy the sensitivity requirements of the 5D hyperchaotic system, a rounding operator is implemented to restrict all updated positions to a precision of three decimal places 10^{-3}. During the evaluation phase, the fitness of each particle (defined by the KYD D_{ky}) is calculated using the Wolf algorithm. If the current position $x_i(t+1)$ yields a better D_{ky} than the $pbest_i$, the personal best is updated. Furthermore, the swarm identifies the global best gbest among all personal bests. The PSO algorithm continues to iterate until the maximum number of generations is reached, at which point the optimal parameters [a, b, d, k] and the maximum D_{ky} are retrieved.

6.3. Results and discussion

The initial search intervals for the system parameters are established based on the preliminary dynamical analysis presented in Section 3. The parameter ranges for [a, b, d, k] are defined as follows: $a \in$ in [6, 8], $b \in$ [40, 60], $d \in$ [0.15, 0.3], and $k \in$ [-0.4, 0]. These bounds are critical to ensure that the optimization algorithms focus on regions exhibiting potential hyperchaotic behavior, rather than periodic or divergent dynamics. For a fair comparison, both algorithms are executed using the same configuration, with a population size of 30 individuals and a total of 20 generations. Results are shown in Table 3.

Table 3. Comparison of PSO and DE performance in terms of local DKY and MLE across generations.

Generation	**PSO**		**DE**	
	Local best D_{ky}	**Local best MLE**	**Local best D_{ky}**	**Local best MLE**
1	4.1246	0.8884	4.1381	0.9296
2	4.1316	0.8623	4.1445	0.9867
3	**4.1375**	**0.9262**	4.1452	0.9938
4	4.1373	0.9266	4.1331	0.8870
5	4.1374	0.9218	4.1365	0.9115
6	4.1339	0.9176	4.1380	0.9398
7	4.1345	0.9899	4.1369	0.9224
8	4.1344	0.9078	4.1367	1.0021
9	4.1364	0.9293	4.1132	0.8805
10	4.1340	0.8992	4.1453	0.9993
11	4.1362	0.9044	4.1397	0.9245
12	4.1351	0.9032	4.1388	0.9339
13	4.1346	0.9094	4.1448	1.0041
14	4.1366	0.9217	4.1441	0.9953
15	4.1368	0.9184	**4.1509**	**1.0414**
16	4.1348	0.9171	4.1454	1.0151
17	4.1351	0.9206	4.1447	0.9944
18	4.1657	0.9243	4.1448	0.9875
19	4.1346	0.9021	4.1509	1.0430
20	4.1347	0.9172	4.1461	0.993

The comparative study between DE and PSO reveals that DE is more effective in maximizing the topological complexity of the proposed 5D system. While PSO demonstrates rapid convergence during the early generations, it converges prematurely to a lower global optimum. As shown in Table 4, the DE algorithm successfully identifies the parameter set [6.000, 60.000, 0.283, -0.189], which outperforms the solution obtained by PSO. The optimization process leads to an increase in the fractal dimension and the LEs. According to the results presented in Table 4, the DE algorithm achieves an optimal KYD D_{ky} of 4.150879, representing the highest topological complexity identified for the new system, surpassing the results reported in Table 2. This high D_{ky} value is supported by an optimized Lyapunov spectrum exhibiting three positive exponents, with an MLE of 1.0414.

Table 4. Optimal parameters, maximized Kaplan-Yorke dimension, and Lyapunov Exponents (LEs) spectrum for the new 5D system using DE and PSO algorithms.

Algorithm	Optimal parameters	Optimal D_{ky}	LEs
DE	a =6.000, b = 60.000, d = 0.283, k = -0.189	4.150879	1.0414, 0.0795, 0.0566, 0.0055, -7.8410
PSO	a=6.000, b= 50.000, d=0.209, k= -0.152	4.137453	0.9262, 0.0890, 0.0493, 0.0064, -7.7917

7. 0-1 test and approximate entropy

In this section, we provide a comparative complexity analysis of the 3D Dong system, 4D Dong system, and the proposed 5D hyperchaotic system across four distinct parameter sets (S1–S4). The complexity is quantified using the robust 0-1 test for chaos K-value and Approximate Entropy (ApEn), calculated using the y-coordinate over a simulation time of t = 2000s to ensure statistical convergence. The 0-1 test distinguishes regular and chaotic dynamics, where a K-value approaching 1 confirms the existence of chaos [35]. Furthermore, ApEn measures the unpredictability and regularity of the time series, with higher values indicating a more complex and unpredictable system [36]. The comparative results are summarized in the Table 5.

Table 5. Complexity results (K-value and ApEn) for different systems using y-coordinate at t = 2000s for {S1, S2, S3, S4} = {(8, 50, 0.2, −0.2), (8, 48, 0.2, -0.2), (6, 50, 0.209, -0.152), and (6, 60, 0.283, -0.189)}.

System	Parameters	K value	ApEn
3D Dong	as in [23]	0.9958	0.4958
4D Dong	as in [22]	0.9961	0.5624
	S1: Construction parameters	0.9971	0.7628
5D System	S2: High D_{ky} in Table 2	0.9978	0.7616
	S3: PSO Optimized	0.9980	0.8114
	S4: DE Optimized	0.9985	0.8242

For all investigated systems and parameter sets, the K-value remains very close to 1 ($K > 0.99$), confirming that the systems operate in a fully chaotic regime. In addition, the results reveal a correlation between system dimensionality and dynamical complexity. The 5D hyperchaotic system consistently exhibits higher Approximate Entropy (ApEn) values compared to the 3D and 4D Dong systems. For example, the ApEn value of the 5D system for S1 (0.7628) is approximately 53% higher than that of the 3D system (0.4958), indicating a significantly greater level of signal unpredictability and structural richness.

Furthermore, the optimization of the 5D system parameters leads to an additional increase in complexity. The parameter set S4 (obtained using DE) achieves the highest overall complexity, with K = 0.9985 and ApEn = 0.8242. This observation is consistent with the complexity analysis, where S4 was identified as exhibiting the most pronounced hyperchaotic behavior.

Finally, the increase in ApEn from S1 to S4 confirms that the optimization techniques (PSO and DE) successfully identify regions of the parameter space associated with higher dynamical complexity. Consequently, the parameter set S4 is recommended for applications such as pseudo-random number generation (PRNG) and chaos-based secure communication schemes, where enhanced unpredictability and complexity are critical.

8. Conclusions

In this work, we have constructed a new five-dimensional hyperchaotic system from Dong's original 3D chaotic model and its four-dimensional hyperchaotic extension. Adding a linear feedback controller and a fifth state variable to the 4D system, and adjusting the parameter set, we were able to create a system that is hyperchaotic with three positive LEs. Through numerical simulations, we described the complex dynamics of the model, distinguishing periodicity, chaos, and hyperchaos regions. The use of LE spectra, KYD, and phase portraits showed the system's high complexity. We also demonstrated that multistability is an intrinsic feature of the model, with different initial conditions leading to distinct coexisting attractors even for fixed parameters. We have also employed an offset boosting control mechanism to show that the attractors can be shifted along the u-direction without influencing the intrinsic dynamics of the system. Moreover, a topological complexity optimization framework based on Particle Swarm Optimization (PSO) and Differential Evolution (DE) was used to maximize the Kaplan–Yorke dimension, followed by validation using the 0–1 test and Approximate Entropy analysis. These features enhance unpredictability and qualify the system to be used in secure communications and cryptography. In future work, we will focus on developing image encryption and secure signal transmission schemes based on the proposed 5D hyperchaotic system.

Author contributions

Khaled Benkouider: Writing–original draft preparation, methodology, software; Mohammed A. Saleh: Funding acquisition, writing–review and editing, software; Aceng Sambas: Conceptualization, methodology, formal analysis; Sulaiman M. Ibrahim: Optimization, investigation, writing–original draft preparation; Abdulgader Z. Almaymuni: Funding acquisition, writing–review and editing, software; Badr Almuturi: Formal analysis, data curation, writing–review and editing; D. Iranian: Formal analysis, data curation, writing–review and editing. All authors reviewed the results and approved the final version of the manuscript.

Use of Generative-AI tools declaration

The authors declare they have not used Artificial Intelligence (AI) tools in the creation of this article.

Funding

The Researchers would like to thank the Deanship of Graduate Studies and Scientific Research at Qassim University for financial support (QU-APC-2026).

Conflicts of interest

The authors declare no conflicts of interest to report regarding the present study.

References

1. S. Wang, J. He, Design of new chaotic system with multi-scroll attractor by using variable transformation and its application, *Phys. Scripta*, **100** (2025), 025230. https://doi.org/10.1088/1402-4896/adaa39
2. P. Ding, P. Geng, W. Hu, A new controllable multi-wing chaotic system: Applications in high-security color image encryption, *J. Supercomput.*, **81** (2025), 108. https://doi.org/10.1007/s11227-024-06635-3
3. A. Tiwari, P. Diwan, T. D. Diwan, M. Miroslav, S. P. Samal, A compressed image encryption algorithm leveraging optimized 3D chaotic maps for secure image communication, *Sci. Rep.*, **15** (2025), 14151. https://doi.org/10.1038/s41598-025-95995-8
4. A. Sambas, W. S. M. Sanjaya, M. Mamat, R. P. Prastio, *Mathematical modelling of chaotic jerk circuit and its application in secure communication system*, In: Advances in chaos theory and intelligent control, **337** (2016), 133–153. https://doi.org/10.1007/978-3-319-30340-6_6
5. W. Feng, Z. Tang, X. Zhao, Z. Qin, Y. Chen, B. Cai, et al., State-dependent variable fractional-order hyperchaotic dynamics in a coupled quadratic map: A novel system for high-performance image protection, *Fractal Fract.*, **9** (2025), 792. https://doi.org/10.3390/fractalfract9120792
6. S. Deng, J. Jin, Z. Li, C. Chen, F. Yu, A MBPAF-memristive hopfield neural network and its application in image encryption, *Cogn. Neurodynamics*, **20** (2026), 81. https://doi.org/10.1007/s11571-026-10449-9
7. Y. Alloun, M. S. Azzaz, A. Kifouche, A new approach based on artificial neural networks and chaos for designing deterministic random number generator and its application in image encryption, *Multimed. Tools Appl.*, **84** (2025), 5825–5860. https://doi.org/10.1007/s11042-024-19136-5
8. F. Sun, Z. Lv, C. Wang, Pseudo-random number generation based on spatial chaotic map of Logistic type and its cryptographic application, *Int. J. Mod. Phys. C*, **36** (2025), 2450172. https://doi.org/10.1142/S0129183124501729
9. A. Sambas, W. S. M. Sanjaya, M. Mamat, O. Tacha, Design and numerical simulation of unidirectional chaotic synchronization and its application in secure communication system, *J. Eng. Sci. Tech. Rev.*, **6** (2013), 66–73.

10. Z. Kotadai, C. Fischer, J. D. R. Muñoz, E. T. Cuautle, E. J. Yves, Multistability and initial-offset boosting dynamics in a new 3D memristive chaotic system with FPGA implementation, *Eur. Phys. J. Plus.*, **139** (2024), 70. https://doi.org/10.1140/epjp/s13360-024-04859-z
11. E. J. Mendoza, G. Z. Mejia, E. T. Cuautle, A. D. Sánchez, CMOS design of a chaos-based masking system for biomedical signals applications, *Int. J. Circ. Theor. App.*, **53** (2025), 5802–5815. https://doi.org/10.1002/cta.4500
12. E. N. Lorenz, Deterministic non-periodic flow, *J. Atoms. Sci.*, **20** (1963), 130–141. https://doi.org/10.1175/1520-0469(1963)020%3C0130:DNF%3E2.0.CO;2
13. E. Igra, Knots and chaos in the Rössler system, *J. Differ. Equations*, **437** (2025), 113290. https://doi.org/10.1016/j.jde.2025.113290
14. X. Lu, Y. Liu, A. Liu, C. Feng, New geometric viewpoints to Chen chaotic system, *Miskolc Math. Notes.*, **23** (2022), 339–362. https://doi.org/10.18514/MMN.2022.3787
15. S. M. S. Rana, M. J. Uddin, Dynamics of a discrete-time chaotic Lü system, *Pan-Amer. J. Math.*, **1** (2022), 7. https://doi.org/10.28919/cpr-pajm/1-7
16. Z. Zheng, Z. Chen, B. Long, T. Liu, X. Wu, X. Deng, et al., Multi-strategy color image encryption scheme based on compressed sensing and a novel 4D hyperchaotic system, *Nonlinear Dynam.*, **113** (2025), 28275–28304. https://doi.org/10.1007/s11071-025-11516-2
17. X. Zhang, H. Zhang, A novel image encryption scheme using both pixel-level and bit-level permutations with an improved hyperchaotic system, *Cluster Comput.*, **28** (2025), 388. https://doi.org/10.1007/s10586-024-05007-z
18. M. Mechekef, L. Meddour, T. Houmor, Generation of a multiwing hyperchaotic system with a line equilibrium and its control, *J. Comput. Nonlin. Dyn.*, **20** (2025), 041007. https://doi.org/10.1115/1.4067860
19. T. Zhao, Y. Wei, X. Wang, X. Sun, B. Du, A novel conservative grid multi-scroll hyperchaotic system with two-parameter regulation, *Eur. Phys. J. Plus.*, **140** (2025), 566. https://doi.org/10.1140/epjp/s13360-025-06487-7
20. Q. Yang, L. Yang, B. Ou, Hidden hyperchaotic attractors in a new 5D system based on chaotic system with two stable node-foci, *Int. J. Bifurcat. Chaos*, **29** (2019), 1950092. https://doi.org/10.1142/S0218127419500925
21. S. F. Al-Azzawi, A. M. Hasan, New 5D hyperchaotic system derived from the sprott C system: Properties and anti synchronization, *J. Intell. Syst. Control*, **2** (2023), 110–122. https://doi.org/10.56578/jisc020205
22. C. Dong, J. Wang, Hidden and coexisting attractors in a novel 4D hyperchaotic system with no equilibrium point, *Fractal Fract.*, **6** (2022), 306. https://doi.org/10.3390/fractalfract6060306
23. C. Dong, Dynamics, periodic orbit analysis, and circuit implementation of a new chaotic system with hidden attractor, *Fractal Fract.*, **6** (2022), 190. https://doi.org/10.3390/fractalfract6040190
24. A. Wolf, J. B. Swift, H. L. Swinney, J. A. Vastano, Determining LEs from a time series, *Physica D*, **16** (1985), 285–317. https://doi.org/10.1016/0167-2789(85)90011-9
25. F. Yu, S. Xu, X. Xiao, W. Yao, Y. Huang, S. Cai, et al., Dynamic analysis and FPGA implementation of a 5D multi-wing fractional-order memristive chaotic system with hidden attractors, *Integration*, **96** (2024), 102129. https://doi.org/10.1016/j.vlsi.2023.102129
26. C. Dong, M. Yang, Extreme homogeneous and heterogeneous multistability in a novel 5D memristor-based chaotic system with hidden attractors, *Fractal Fract.*, **8** (2024), 266. https://doi.org/10.3390/fractalfract8050266

27. Z. Zhuang, Z. Zhuang, T. Wang, Medical image encryption algorithm based on a new five-dimensional multi-band multi-wing chaotic system and QR decomposition, *Sci. Rep.*, **14** (2024), 402. https://doi.org/10.1038/s41598-023-50661-9
28. M. D. Johansyah, K. Benkouider, S. Vaidyanathan, A. Sambas, C. Aruna, A new 5D chaotic supply chain system with transport lag: Modeling, bifurcation analysis, offset boosting control and synchronization, *Mathematics*, **13** (2025), 3560. https://doi.org/10.3390/math13213560
29. L. J. Sagban, A. A. Shukur, Dynamics and adaptive control of a novel 5d hyperchaotic system: Either hidden attractor or self-excited with unusual nature of unstable equilibria, *Malays. J. Math. Sci.*, **18** (2024), 675–696. https://doi.org/10.47836/mjms.18.3.14
30. C. Xiu, J. Fang, Y. Liu, Design and circuit implementation of a novel 5D memristive CNN hyperchaotic system, *Chaos Soliton. Fract.*, **158** (2022), 112040. https://doi.org/10.1016/j.chaos.2022.112040
31. D. Khattar, N. Agrawal, M. Sirohi, Dynamical analysis of a 5D novel system based on Lorenz system and its hybrid function projective synchronisation using adaptive control, *Pramana-J. Phys.*, **97** (2023), 76. https://doi.org/10.1007/s12043-023-02544-x
32. H. Niu, Analysis and stability control of a novel 5D hyperchaotic system, *J. Robot. Netw. Artif. L.*, **8** (2022), 245–248. https://doi.org/10.2991/jrnal.k.211108.003
33. S. Shi, H. Lu, C. Du, Z. Zhang, L. Liu, Analysis and application of a 3D chaotic system with an extremely extensive range of amplitudes and offset boosting, *Phys. Scripta*, **100** (2025), 025209. https://doi.org/10.1088/1402-4896/ada11b
34. M. F. M. López, A. J. L. Martinez, A. M. G. Zapata, A. S. Juarez, L. G. D. L. Fraga, E. T. Cuautle, FPGA implementation of PRNGs based on chaotic systems optimized by DE, GWO, and PSO, *Int. J. Circ. Theor. App.*, **53** (2025), 5875–5892. https://doi.org/10.1002/cta.4435
35. D. Bernardini, G. Litak, An overview of 0–1 test for chaos, *J. Braz. Soc. Mech. Sci.*, **38** (2016), 1433–1450. https://doi.org/10.1007/s40430-015-0453-y
36. A. D. Bonal, A. Marshak, Approximate entropy and sample entropy: A comprehensive tutorial, *Entropy*, **21** (2019), 541. https://doi.org/10.3390/e21060541